Narrow Field-of-View Radiometer (NFOV) Handbook

November 2008

C. Chiu
A. Marshak
G. Hodges
J.C. Barnard
J. Schmelzer

Contents

Figures

Tables

1. General Overview

The two-channel narrow field-of-view radiometer (NFOV2) is a ground-based radiometer that looks straight up and measures radiance directly above the instrument at wavelengths of 673 and 870 nm. The field-of-view of the instrument is 1.2°, and the sampling time resolution is one second. Measurements of the NFOV2 have been used to retrieve optical properties for overhead clouds that range from patchy to overcast. With a one-second sampling rate of the NFOV2, faster than almost any other ARM Climate Research Facility (ACRF) instrument, we are able, for the first time, to capture changes in cloud optical properties at the natural time scale of cloud evolution.

Note that ACRF had a one-channel narrow field-of-view (NFOV) radiometer that provided valuable measurements for further developing the NFOV2. More details about the NFOV can be found in Section 3.

2. Contacts

2.1 Mentor

Gary Hodges
Phone: 303-497-6460
Gary.Hodges@noaa.gov

Christine Chiu
Phone: 301-614-6213
Christine.Chiu@nasa.gov

2.2 Instrument Developer

James Barnard
Pacific Northwest National Laboratory
(509) 372-6145
james.barnard@pnl.gov

John Schmelzer, Retired

Warren Wiscombe
Brookhaven National Laboratory
Phone: (631) 344-4260
wwiscomb@bnl.gov

Alexander Marshak
Phone: (301) 614-6122
Alexander.Marshak@nasa.gov

3. Deployment Locations and History

The narrow field-of-view radiometer was designed as a fast (sampling rate of 1 Hz), simple, cheap instrument to measure clouds, and complement the radars, lidars, and microwave radiometers by having a

similar narrow field-of-view (5.7°). To minimize molecular (Rayleigh) scattering, measurements of the instrument were taken at a wavelength of 870 nm, and thus the instrument was called one-channel narrow field-of-view radiometer (NFOV). The NFOV worked well until being damaged during a storm in June 2002, and had been decommissioned since June 2007.

Unlike flux instruments, the NFOV that measures zenith radiance has the potential to provide local estimates of cloud optical depth. However, there are two major problems with retrieving cloud optical depth from monochromatic zenith radiance. First, in one-dimensional (1D) plane-parallel radiative transfer theory, the relationship between solar zenith radiance and cloud optical depth is not a one-to-one function (as shown in Figure 1). Therefore, unambiguously determining the optical depth from radiance measured by a one-channel radiometer is nearly impossible. Second, the histogram of actual observations (solid line in Figure 1) from the NFOV reveals that, due to three-dimensional (3D) effects, some radiance values may exceed those permitted by 1D models. This results in cloud optical depth being irretrievable for those zenith radiances.

Because of the aforementioned problems, a second channel at 673 nm was added to the new instrument, NFOV2. The NFOV2 was deployed at the ACRF Southern Great Plains (SGP) site in September 2004. Soon the NFOV2 became one of the main radiometers of the ARM Mobile Facility (AMF) with deployments in June–September 2005 at Point Reyes, California, and at the Black Forest of Germany in 2007. The NFOV2 was also in China with the AMF for the study of aerosol indirect effects.
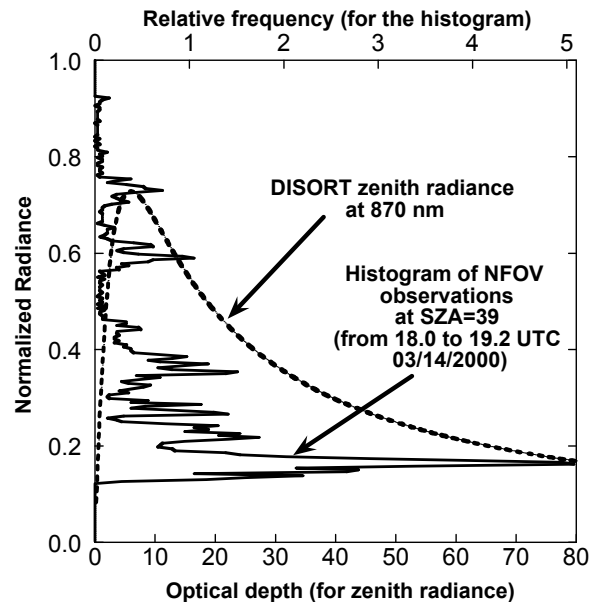
Figure 1. Downward 870-nm radiances vs. cloud optical depth (lower x-axis) calculated by the 1D radiative transfer model DISORT (Stamnes et al., 1988) with a surface albedo of 0.271. Co-plotted solid curve is a histogram (upper x-axis) of NFOV 870-nm radiances measured at the ACRF Oklahoma site from 18 to 19.2 UTC, March 14, 2000.

When the NFOV2 was deployed at the SGP site, it had the same a field-of-view as NFOV (5.7°). However, it was found that incorrect cloud optical depths would be retrieved when the instrument's FOV was filled with both clouds and clear-sky. To lower the amount of clear-sky contaminations (Chiu et al.,

2006), the FOV was then reduced to 1.2°, which had the side benefit of matching the fields-of-view of both the ACRF shortwave spectrometer and the National Aeronautics and Space Administration (NASA) Aerosol Robotic Network (AERONET) sun photometers.

4. Near-Real-Time Data Plots

Data plots are available from the DQ Hands Plot Browser for the AMF deployments (FKB and HFE).

5. Data Description and Examples

5.1 Data File Contents

This section is under development.

5.1.1 Primary Variable and Expected Uncertainty

The primary variables measured by NFOV radiometers are the:

- Zenith radiance at 673 nm (Wm-2sr-1nm-1)
- Zenith radiance at 870 nm (Wm-2sr-1nm-1).

5.1.1.1 Definition of Uncertainty

5.1.2 Secondary Underlying Variables

Additional Information about variables may be found at ARM netCDF file header descriptions for the NFOV2.

5.1.3 Diagnostic Variables

5.1.4 Data Quality Flags

5.1.5 Dimension Variables

5.2 Annotated Examples

Two examples from the AMF Convective and Orographically-induced Precipitation Study (COPS) experiment are shown in Figure 2. The left panel is for a clear day, and the right panel is for a cloudy day. Total sky images are also shown to display the corresponding cloud fields. Figures 2a and 2d show that due to stronger cloud scattering, observed radiances are much higher on the cloudy day than those on the clear day. For both days, radiances at 673 nm (RED) are larger than those at 870 nm (NIR).

We further normalize zenith radiance measurement $I_{m,\lambda}$ at wavelength λ using:

$$I_\lambda = \frac{\pi \cdot I_{m,\lambda}}{\mu_0 \cdot F_{TOA,\lambda}},$$

$$(1.1)$$

where I_λ is the normalized zenith radiance; $F_{TOA,\lambda}$ is the solar irradiance at the top of the atmosphere; and μ_0 is the cosine of solar zenith angle (SZA). From normalized zenith radiances (Figures 2b and 2e), we see clearly that radiances at NIR are larger than those at RED wavelength for the cloudy day.
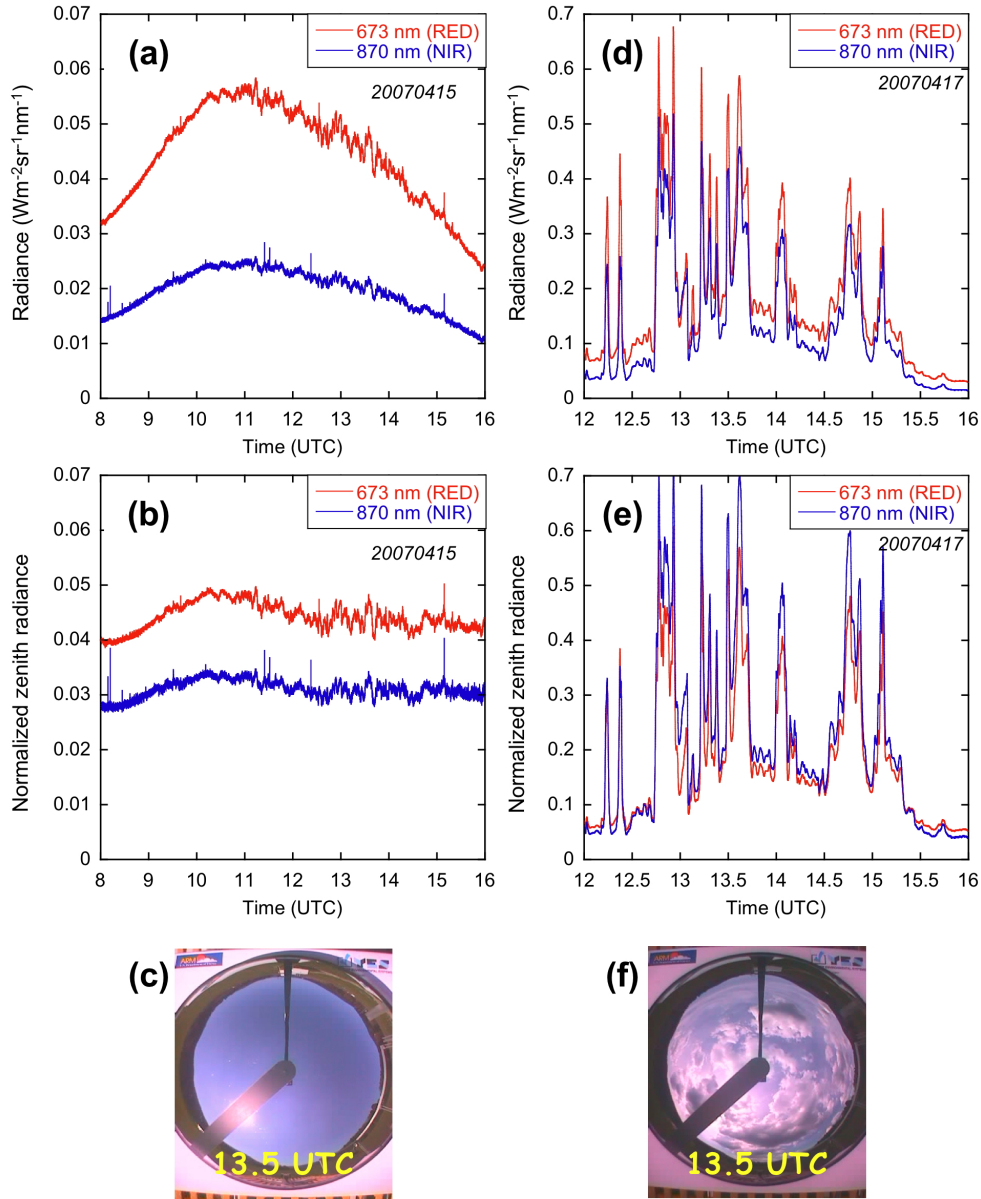

Figure 2. Downward radiances (a) and normalized radiances (b) of the NFOV2 measured at the Black Forest, Germany, on 15 April 2007. A total sky image at 13.5 UTC is shown in (c). (d)–(f) are same as (a)–(c), but for 17 April 2007. Note that values of y-axis for these two days are different by an order.

5.3   User Notes and Known Problems

This section is under development.

4

5.4 Frequently Asked Questions

This section is under development.

6. Data Quality

Calibrations are performed to produce a calibration factor that converts NFOV2 raw detector counts to zenith radiance. The NFOV2 is calibrated at the NASA Goddard Space Flight Center Calibration Facility, using the 36-inch integrating Teflon sphere. The sphere, calibrated several times a year using a spectroradiometer and a secondary lamp standard (http://cf.gsfc.nasa.gov/docs/proc/radcalprocs.pdf), has been used to calibrate all sun photometers of the NASA AERONET. Uncertainties in radiances of the sphere at wavelengths of 673 and 870 nm are typically around 1–3 % (http://cf.gsfc.nasa.gov).

During the calibration process, dart counts and signals for 4, 8, 12, and 16 lamps of the sphere are measured. A calibration factor is then derived from the relationship between signals of the NFOV2 and radiances of the sphere, using a linear regression approach. A final zenith radiance I ($Wm^{-2}sr^{-1}nm^{-1}$) is given as

$$I = aV + b, \tag{1.2}$$

where a is the calibration factor; b is the offset based on nighttime measurements; and V is detector counts. Values of a and b can be found in the header of data files for both 673 and 870 nm wavelengths.

Note that calibrations are performed when the lens of the NFOV2 is clean. However, in the field, raindrops or other deposits (e.g., sea salt, dust, and bird droppings) might contaminate the lens, which will lead to inaccurate measurements. There are two approaches to correct those measurements. First, one can use linear combinations of calibration factors obtained from the pre- and post- experiment. Second, one can use redundant measurements of the AMF sun photometer. Based on data collected in the AMF COPS deployment, measurements of NFOV2 and the sun photometer agree within 2%.

6.1 Data Quality Health and Status

The following links go to current data quality health and status results:

- DQ HandS (Data Quality Health and Status)
- NCVweb for interactive data plotting using.

The tables and graphs shown contain the techniques used by ARM's data quality analysts, instrument mentors, and site scientists to monitor and diagnose data quality.

6.2 Data Reviews by Instrument Mentor

This section is not applicable to this instrument.

6.3 Data Assessments by Site Scientist/Data Quality Office

All DQ Office and most Site Scientist techniques for checking have been incorporated within DQ HandS and can be viewed there.

6.4   Value-Added Procedures and Quality Measurement Experiments

Many of the scientific needs of ARM are met through the analysis and processing of existing data products into "value-added" products or VAPs. Despite extensive instrumentation deployed at the ACRF sites, there will always be quantities of interest that are either impractical or impossible to measure directly or routinely. Physical models using ACRF instrument data as inputs are implemented as VAPs and can help fill some of the unmet measurement needs of the program. Conversely, ARM produces some VAPs not to fill unmet measurement needs, but to improve the quality of existing measurements. In addition, when more than one measurement is available, ARM also produces "best estimate" VAPs. A special class of VAP called a Quality Measurement Experiment (QME) does not output geophysical parameters of scientific interest. Rather, a QME adds value to the input datastreams by providing for continuous assessment of the quality of the input data based on internal consistency checks, comparisons between independent similar measurements, or comparisons between measurement with modeled results, and so forth. For more information, see the VAPs and QMEs web page.

7.   Instrument Details

7.1   Detailed Description

7.1.1   List of Components

The instrument consists of two modules, as shown in Figure 3. The instrument on the left is the NFOV2, while the grey enclosure on the right holds the power supply, the head/tube heater controller, and the Campbell data logger. In Figure 3, two yellow cables connect the NFOV2 and the enclosure. The small cable carries current to the window heater, while the large cable carries the signal, and current to heat the head.
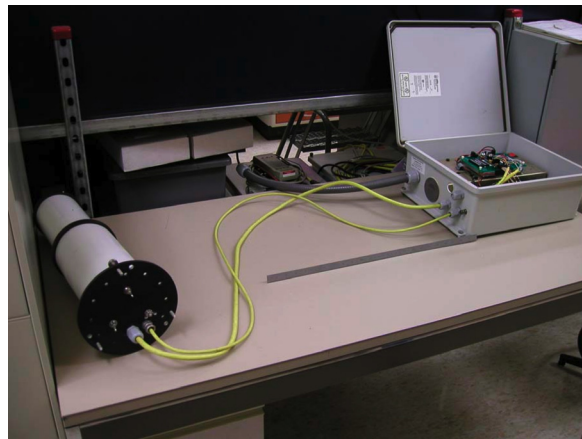

Figure 3.   The NFOV2 (at left) and the enclosure (at right) that contains the power supply and data logger.

Specifications are given as the following:

- Two radiometers:

     NFOV: 1-channel narrow field-of-view radiometer with a filter 870 nm

     NFOV2: 2-channel narrow field-of-view radiometer with filters 673 and 870 nm

- Components:

  The NFOV is comprised of a MFRSR head and a collimator that sits atop the head. The collimator restricts the field of view of the instrument.

- FOV:

  NFOV: 5.7°

  NFOV2: 5.7° and 1.2° prior to and after 2004, respectively.

- Bandwidth: 10 nm at full width at half maximum (response function data)

- Detector: Silicon diode detector

- Data output: The data format from the Campbell data logger is shown in Table 1.

Table 1. Cambell data logger data format.

Column	Descriptions
1	Line number of Campbell code that produces the output
2	Year (e.g., 2008)
3	Julian day
4	Time in HHMM format
5	Time in seconds
6	Output for 870 nm in mV
7	Output for 673 nm in mV
8	Head temperature in mV (this value should be around 1450)
9	Tube temperature in mV (this value should be around 1400)

7.1.2   System Configuration and Measurement Methods

This section is under development.

7.1.3   Specifications

This section is under development.

7.2   Theory of Operation

The NFOV radiometers point straight up. The collimating tube restricts the FOV of the instruments. The detector that resides in the instrument's head senses photons that travel in the right direction and enter the collimator. The detector is an interference filter/Silicon diode detector. The head is kept at a constant temperature (insofar as possible) to prevent temperature effects from influencing the measurements. The sensitivity to head temperature appears to be about a 1% change in radiance for every 1 K change in head temperature.

7.2.1   Retrieval Method for Cloud Optical PropertiesTheory

Cloud optical depth (or thickness) is a fundamental property for calculating the amount of solar radiation entering and leaving Earth's atmosphere. Most techniques to measure this property work well for completely overcast skies, but are inapplicable for broken-cloud skies. Marshak et al. (2004) and Chiu et al. (2006) developed a retrieval method that uses NFOV2 measurements and works for any 3D cloud situation over a vegetated surface. Their method, dubbed REDvsNIR, works because, at 673 nm (RED) and 870 nm (NIR), clouds have nearly identical optical properties while vegetated surfaces reflect quite differently.

The retrieval concept is explained as follows. Consider a plane of normalized zenith radiance at NIR versus that at RED (as shown in Figure 4). For clear-sky situations, due to stronger molecular scattering at shorter wavelengths, radiance at RED is larger than that at NIR wavelengths. Therefore, points below the diagonal in Figure 4 correspond to clear sky. On the contrary, for cloudy situations, radiance at NIR is larger than that at RED wavelengths. The contrast is resulted from stronger surface-cloud interactions at NIR, because vegetated surfaces are bright at NIR wavelengths but dark at red wavelengths. Therefore, points above the diagonal correspond to cloudy situations.

Notice that data points A and B are both above the diagonal line, indicating they correspond to cloudy situations. They have the same RED radiances and thus have the same cloud optical depths. However, they have different radiances at NIR wavelength. A higher radiance at NIR indicates that more surface-cloud interactions occur and more photons reach the ground. It implies that point B has a smaller cloud fraction than point A. As a result, this method retrieves not only cloud optical depth, but also effective cloud fraction.
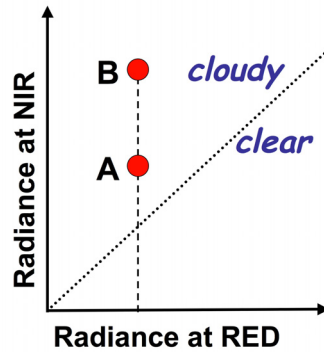

Figure 4. A schematic illustration of the REDvsNIR method for retrieving cloud optical depth and cloud fraction.

The above illustrations can all be made quantitatively in the RED vs NIR method, which retrieves both optical depth τ and effective cloud fraction A_c from a point in the RED vs. NIR plane. We use DISORT (Discrete-Ordinate-method) radiative transfer model to calculate zenith radiance I over a reasonable range of τ and A_c for both channels, given as

$$I_{RED} = I_{RED}(\tau, A_C),$$
$$I_{NIR} = I_{NIR}(\tau, A_C).$$

(1.3)

8

We then build a 2D lookup table based on these calculations. By plotting radiance measurements on the lookup table (as shown in Figure 5), both cloud optical depth and effective cloud fraction can be determined by the underlying lines. Detailed explanations, sensitivity analyses, and discussions about this retrieval method can be found in Marshak et al. (2004) and Chiu et al. (2006).
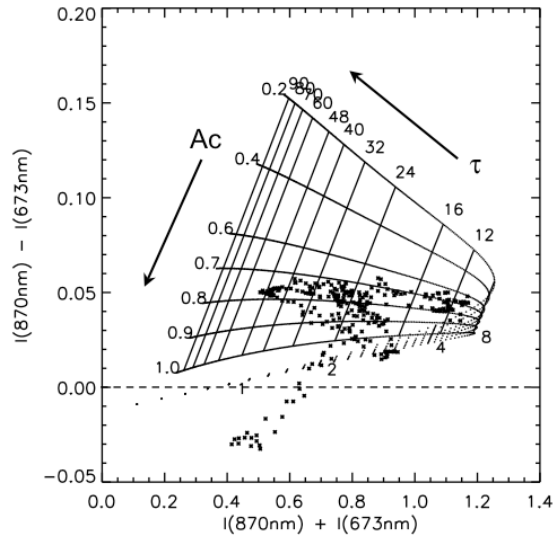

Figure 5. A lookup table (lines) constructed for SZA = 52°, effective radius of 8 μm, and surface albedo values of 0.13 and 0.28 for RED and NIR channels, respectively. Dots are normalized zenith radiance measurements from the ACRF NFOV2 radiometer at the SGP site during 17.2 and 17.28 UTC on October 28, 2004. τ is cloud optical depth and A_c is effective cloud fraction.

7.3   Calibration

This section is under development.

7.3.1   Theory

7.3.2   Procedures

7.3.3   History

7.4   Operation and Maintenance

This section is under development.

7.4.1   User Manual

7.4.2   Routine and Corrective Maintenance Documentation

7.4.3   Software Documentation

7.4.4   Additional Documentation

7.5 Glossary

See [ARM Glossary](#)

7.6 Acronyms

See the [ARM Acronyms and Abbreviations](#)

8. Citable References

Chiu, JC, A Marshak, Y Knyazikhin, WJ Wiscombe, HW Barker, JC Barnard, and Y Luo. 2006. "Remote sensing of cloud properties using ground-based measurements of zenith radiance." *Journal of Geophysical Research* 111: D16201, doi:10.1029/2005JD006843.

Marshak, A, Y Knyazikhin, KD Evans, and WJ Wiscombe. 2004. "The 'RED versus NIR' plane to retrieve broken-cloud optical depth from ground-based measurements, cloud-vegetation interaction: Use of normalized difference cloud index for estimation of cloud optical thickness." *Journal of Atmospheric Science* 61: 1911-1925.

Stamnes, K, S–C Tsay, WJ Wiscombe, and K Jayaweera. 1988. "Numerically stable algorithm for discrete-ordinate-method radiative transfer in multiple scattering and emitting layered media." *Applied Optics* 27: 2502–2512.